

# Surface Melting of the Vortex Lattice in Layered Superconductors: Density Functional Theory

A. De Col<sup>1</sup>, G.I. Menon<sup>2</sup>, V.B. Geshkenbein<sup>1,3</sup>, and G. Blatter<sup>1</sup>

<sup>1</sup>*Theoretische Physik, ETH-Zürich, CH-8093 Zürich, Switzerland*

<sup>2</sup>*The Institute of Mathematical Sciences, C.I.T. Campus, Taramani, Chennai 600 113, India and*

<sup>3</sup>*L.D. Landau Institute for Theoretical Physics RAS, 117940 Moscow, Russia*

(Dated: March 23, 2022)

We study the effects of an *ab*-surface on the vortex-solid to vortex-liquid transition in layered superconductors in the limit of vanishing inter-layer Josephson coupling. We derive the interaction between pancake vortices in a semi-infinite sample and adapt the density functional theory of freezing to this system. We obtain an effective one-component order-parameter theory which can be used to describe the effects of the surface on vortex-lattice melting. Due to the absence of protecting layers in the neighbourhood of the surface, the vortex lattice formed near the surface is more susceptible to thermal fluctuations. Depending on the value of the magnetic field, we predict either a continuous or a discontinuous surface melting transition. For intermediate values of the magnetic field, the surface melts continuously, assisting the formation of the liquid phase and suppressing hysteresis above the melting transition, a prediction consistent with experimental results. For very low and very high magnetic fields, the surface melts discontinuously. The two different surface melting scenarios are separated by two surface multicritical points, which we locate on the melting line.

## I. INTRODUCTION

The melting of the vortex lattice is one of the most remarkable aspects of the phenomenology of the high-temperature superconductors<sup>1,2,3,4,5,6</sup>. Such a melting transition, in common with other discontinuous phase transitions, should involve metastable phases such as an undercooled liquid and an overheated solid. Experiments on the mixed phase in the layered high- $T_c$  superconductor BSCCO however indicate an asymmetric hysteresis at the melting transition<sup>7</sup>, involving a supercooled liquid phase but no overheated solid. In a recent letter<sup>8</sup>, we studied the impact of an *ab*-surface on the vortex lattice melting in layered superconductor and we found that the surface can have a profound effect on the hysteretic behaviour. Our approach combined ideas of density functional theory with a mean-field substrate model proposed in Ref. 9. The present paper provides detailed derivations of the results outlined in Ref. 8. In addition, we present several new results, such as a detailed analysis of the solid-liquid interface and of the multi-critical point at low magnetic fields.

The absence of a metastable solid phase in ordinary solids has been the object of great interest in the literature<sup>10,11,12,13,14,15</sup>. It is now widely accepted that such asymmetric hysteresis can be related to the action of surface (pre-)melting. Surfaces act as a natural nucleation point for the liquid phase and inhibit the appearance of the solid at temperatures above melting. This is due to the fact that the atoms at the surface experience a weaker stabilizing potential. Indeed, the stability analysis for a semi-infinite atom chain<sup>11</sup> shows that the enhanced motion of the first atoms makes the ‘surface’ unstable at a lower temperature with respect to the bulk. This suggests that the surface may represent a favorable nucleation site for the liquid phase. However, criteria based on the stability of the solid phase cannot address

the state of the system beyond the surface instability point.

A comprehensive description of the melting transition in the presence of a surface requires the inclusion of the effects of both the solid and the liquid phases on an equal footing<sup>14,16,17</sup>. On a phenomenological level, this can be done within the framework of Landau theory using the order parameters of the melting transition, i.e., the Fourier components of the particle density. The destabilizing effect of the surface can be accounted for<sup>12,18</sup> by a surface term favoring the appearance of the liquid phase. Following the discussion in Ref. 18, as the simplest example of such a theory one considers a Landau free energy of the type

$$F[\mu] = \int_0^\infty dz \left[ \frac{\ell^2}{2} \left( \frac{d\mu}{dz} \right)^2 + f(\mu) + \ell \delta(z) f_1(\mu) \right], \quad (1)$$

where  $z$  is the distance from the surface,  $\mu$  the ( $z$ -dependent) order parameter and  $f(\mu)$  and  $f_1(\mu)$  the bulk free energy and surface destabilizing potential respectively. For a bulk first-order phase transition with an unstable surface we can choose a form

$$\begin{aligned} f(\mu) &= (a/2)\mu^2 - (b/3)\mu^3 + (c/4)\mu^4, \\ f_1(\mu) &= (a_1/2)\mu^2, \end{aligned}$$

where the coefficients  $a, b, c$  are chosen to be strictly positive and temperature independent, whilst temperature enters in  $a(T)$  via the usual Ansatz for a first-order phase transition  $a(T) - a_m \propto T - T_m$ , with  $T_m$  the melting temperature and  $a_m = 2b^2/9c$ .

The bulk free energy  $f$  shows two minima: one at  $\mu_l = 0$  (liquid) with energy  $f_l = 0$  and a second one at  $\mu_s > 0$  (solid), whose energy depends on temperature. The liquid is the stable minimum above the bulk transition temperature  $T_m$ , while below  $T_m$  the solid becomes the

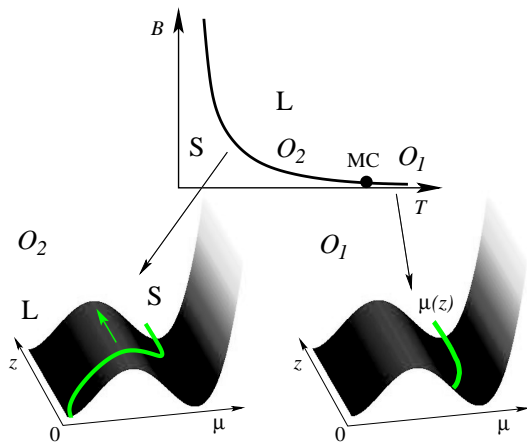


FIG. 1: Top: schematic phase diagram of the pancake vortex system. The multicritical point (MC) separates the portion of the melting line where the surface melts continuously,  $O_2$  transition (left), from the region where the surface melts discontinuously,  $O_1$  transition (right). Lower left: configuration of the order-parameter profile  $\mu(z)$  for an  $O_2$  transition at the melting temperature  $T_m$ . In the language of Landau theory we use in the paper, the problem maps to the determination of the minimal energy configuration of an elastic string,  $\mu(z)$ , subject to a three-dimensional potential landscape, which is described by the bulk free energy, plus an additional surface term, which pushes the tip of the string towards the liquid minimum. In an  $O_2$  transition the surface promotes the formation of the liquid phase upon approaching  $T_m$  from below. The order-parameter profile reaches the liquid minimum continuously at the surface for  $T \nearrow T_m$ , while it remains in the ‘solid’ well in the bulk. The liquid propagates continuously from the surface into the bulk, thus removing the solid phase. Lower right: configuration of the order-parameter profile in an  $O_1$  transition at melting. The order parameter reaches a finite value on the surface at  $T_m$ . Melting occurs via a finite jump for all  $z$  and the solid phase can be overheated.

stable phase. At the transition the two minima assume the same energy and the two phases can coexist.

In the absence of a surface term, the stable configuration is given by a constant order parameter profile throughout the sample. However, the surface free energy  $f_1$  breaks the invariance of the system along  $z$  and pushes the tip of the order parameter profile towards the liquid minimum at  $\mu_1 = 0$ . This term competes with the elastic energy term  $\propto (d\mu/dz)^2$ . A quantitative understanding of the surface destabilization requires to solve the saddle-point equation for the free energy (1). The Euler-Lagrange equation provides the differential equation

$$\ell^2 \frac{d^2 \mu(z)}{dz^2} = \frac{\partial f(\mu(z))}{\partial \mu(z)} \quad (2)$$

which has to be supplemented with the boundary condition originating from the surface term,

$$\ell \left. \frac{d\mu(z)}{dz} \right|_{z=0} = \left. \frac{\partial f_1(\mu(z))}{\partial \mu} \right|_{\mu(z=0)} = a_1 \mu(z=0). \quad (3)$$

Two qualitatively different scenarios are possible depending on the strength of the surface term or, more precisely<sup>18</sup>, on the ratio  $a_1^2/a_m$ . For relatively large perturbations ( $a_1^2/a_m \gg 1$ ) the surface assists the formation of the liquid at the melting transition. Approaching  $T_m$  from below, the bulk order parameter remains in the ‘solid’ well (see Fig. 1), while at the surface the order parameter approaches the liquid minimum at the transition temperature *continuously*. The liquid phase then propagates from the surface and the overheated solid is removed above  $T_m$ . Thus, even if the order parameter in the bulk jumps discontinuously, the surface melts continuously; as the transition is second order at the surface, in Ref. 18 it is referred to as an  $O_2$  transition. On the other hand, when the surface free energy is weak ( $a_1^2/a_m \ll 1$ ), the order parameter at the surface jumps *discontinuously* to the liquid minimum across the transition as in the bulk, although from a reduced value (see Fig. 1). In Ref. 18, this discontinuous surface melting is called an  $O_1$  transition since the transition is first order at the surface. In this case, the surface does not inhibit the appearance of an overheated solid phase.

In this paper, we determine the effects of the surface on the melting of the vortex system, starting from a ‘microscopic’ theory which accounts for the modification of the inter-vortex interactions at the surface. Our program is to derive an appropriate Landau-type free energy similar to Eq. (1) by considering a coarse grained theory where the modulation of the thermally averaged vortex density plays the role of the order parameter. The Density Functional Theory (DFT) of freezing<sup>19</sup> provides an appropriate tool for such a study as it is based on the change of the free energy from a uniform liquid to a modulated state<sup>4,17,20,21,22,23</sup>. The only input which is needed in the analysis is the direct correlator, which we derive within the substrate model approach<sup>9</sup>. Restricting ourselves to periodic modulations, one obtains a free-energy functional in terms of the Fourier component of the pancake vortex density at the first reciprocal lattice vectors of the ordered lattice. Since these are the natural order parameters of the melting transition, the DFT approach provides a microscopic derivation of a Landau type description of the transition similar to Eq. (1).

As a result of our DFT analysis, we find that for very low and very high magnetic fields the surface order-parameter still undergoes a finite, although reduced, jump at the transition ( $O_1$ ). On the other hand, for intermediate values of  $B$ , stray magnetic fields destabilize the layers close to the surface, leading to a continuous transition at the surface ( $O_2$ ). Consequently, for a wide range of experimentally accessible fields we expect that surface fluctuations are sufficiently strong to assist the smooth propagation of the liquid phase into the bulk and to prevent the appearance of the metastable overheated solid phase; this result is consistent with the experiments of Soibel *et al.*<sup>7</sup>. The surface continuous and discontinuous transitions are separated by a multi-critical point. While a precise location of the high-field multi-critical

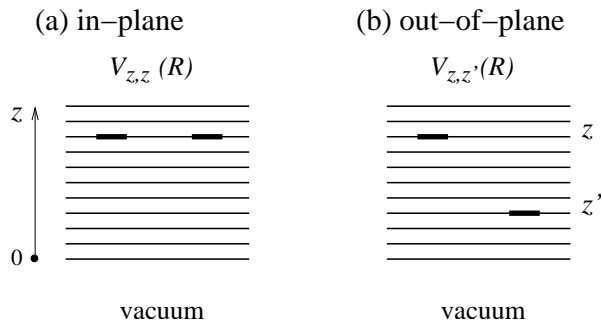


FIG. 2: Geometry of the model studied in the paper. A layered superconductor fills the half space with  $z > 0$ . The interaction between two pancake vortices is affected by the semi-infinite geometry and by the strong anisotropy, leading to a strong logarithmic repulsion between pancake vortices which reside within the same layer (a) or to a weak logarithmic repulsion between pancake vortices in different layers (b).

point goes beyond the limit of validity of our analysis, we have located the low-field multi-critical point by means of an analytical solution of the DFT equations. This analysis is further confirmed numerically.

The paper is organized as follows: we begin by calculating the modified in-plane and out-of-plane pancake vortex interactions (Section II) for a semi-infinite system. In Section III, we review the classic DFT of freezing and derive a specific functional which describes the vortex system in a layered superconductor. We briefly describe the results of the novel DFT-substrate approach for an infinite (bulk) system (Section IV), where other results are available for comparison. We turn to the problem with the surface in Section V, where we present an analytical solution of the problem and show that depending on the value of the magnetic field the system exhibits either a ‘surface non-melting’ ( $O_1$ ) or a ‘surface melting’ ( $O_2$ ) behavior. Finally, in Section VI we confirm the validity of our analytical approach by a direct numerical solution of the DFT equations.

## II. MODEL

We consider a semi-infinite geometry with the superconductor filling the upper half-space  $z \geq 0$  and describe the vortex system within the London theory (see Fig. 2). We model the system as a stack of two-dimensional superconducting layers of thickness  $d_s$ , separated by a distance  $d$ , and with a penetration depth  $\lambda_s$ . We work in the limit of vanishingly small Josephson coupling. The basic topological defects are pancake vortices<sup>24,25</sup> which consist of vortices with a two dimensional core limited to a single superconducting layer.

The vortex interaction is mediated by currents set up by the vortices via the Lorentz force. A finite sheet current  $\mathbf{j}$  acts on the vortex core, producing a perpendicular

force

$$\mathbf{F} = (\Phi_0/c) \mathbf{z} \times \mathbf{j}. \quad (4)$$

To obtain the force between two vortices, one needs the sheet supercurrent generated by any of the two at the location of the core of the other one; then, the interaction is found by integrating the force (4) on the radial coordinate back from infinite distance. The circular current defining a vortex is induced by the  $2\pi$  twist of the phase  $\varphi$  of the complex order parameter  $\psi = |\psi|e^{i\varphi}$ ,

$$\mathbf{j} = -\frac{cd_s}{4\pi\lambda_s^2} \left( \frac{\Phi_0}{2\pi} \nabla\varphi + \mathbf{A} \right). \quad (5)$$

The vector potential  $\mathbf{A}$  screens the action of the driving term  $\nabla\varphi = -\mathbf{n}_z \times \mathbf{R}/R^2$ , annihilating its action when an entire flux quantum  $\Phi_0$  is accumulated. This is the case for Pearl vortices in a single superconducting film which trap an entire flux  $\Phi_0$  at a distance  $\lambda_{\text{eff}} = \lambda_s^2/d$ . However, in the case of layered systems<sup>24,26,27,28</sup>, the presence of other layers reduces the ability of the vortex to bind a full flux quantum and hence the action persists to infinity.

A central quantity in the discussion of the vortex-vortex interaction is the vector potential field  $\mathbf{A}$  produced by a pancake vortex placed in a semi-infinite sample. In the London approximation, a pancake vortex placed at  $z'$  generates a vector potential satisfying the following set of equations

$$\begin{aligned} \nabla^2 \mathbf{A} - \frac{1}{\lambda^2} \mathbf{A} &= \frac{d}{\lambda^2} \nabla\varphi \delta(z - z'), \quad z > 0, \\ \nabla^2 \mathbf{A} &= 0, \quad z < 0. \end{aligned} \quad (6)$$

Note that Eqs. (6) are symmetric with respect to  $z \leftrightarrow z'$ . In (6) we treat the layered system within a continuum approximation, neglecting small modulations in  $\mathbf{A}$  (of sub-leading order  $\sim d/\lambda$ ) across the layers. Such a description is consistent once the layer thickness  $d_s$  and the material penetration depth  $\lambda_s$  are replaced by the inter-layer spacing  $d$  and the bulk penetration depth  $\lambda^2 = \lambda_s^2 d/d_s$ , respectively. By solving Eq. (6), we obtain the vector potential at the point  $(R, z)$  inside the superconductor produced by a pancake vortex placed at the origin of the layer at  $z'$ ,

$$\begin{aligned} A_\phi(R, z \geq 0, z' \geq 0) &= \frac{\Phi_0 d}{2\lambda^2} \int_0^{+\infty} \frac{dK}{2\pi} \frac{J_1(KR)}{K_+} \\ &\times [f_{z-z'}(K) + \beta(K)f_{z+z'}(K)], \end{aligned} \quad (7)$$

with  $f_z(K) = \exp(-K|z|)$  and  $\beta(K) = (K_+ - K)/(K_+ + K)$  (due to the cylindrical symmetry of (6), the vector potential has only an azimuthal component, i.e., along the direction of the unit vector  $\mathbf{n}_\phi = \mathbf{n}_z \times \mathbf{R}/R^2$ ). A convenient quantity, which we will use in the following discussion, is the total flux  $\Phi_t(z, z')$  trapped in the layer at  $z$  due to a pancake vortex placed at a distance  $z'$  from the surface; Eq. (7) provides the result

$$\Phi_t(z, z') = \frac{\Phi_0 d}{2\lambda} \left( e^{-|z-z'|/\lambda} + e^{-(z+z')/\lambda} \right). \quad (8)$$

In the following, we will make use of these results to derive the pancake vortex interaction between co-planar vortices (next subsection) and vortices in different layers (Sect. II B).

### A. In-plane interaction

We first consider two pancake vortices residing on the same layer, cf. Fig. 2(a). Their interaction includes the contributions from both terms in Eq. (5), the driving source  $\nabla\varphi$  and the vector potential  $\mathbf{A}$ . While the phase produces currents decreasing  $\propto 1/R$ , magnetic screening is effective at scales larger than the penetration depth  $\lambda$ . To leading order, the vector potential can be written in terms of the trapped magnetic flux  $\Phi_t(z) \equiv \Phi_t(z, z)$  which threads the layer where the vortex resides:  $A_\phi(R \gg \lambda, z, z) \approx \Phi_t(z)/2\pi R$ . Combining Eqs. (4) and (5), we can extract the in-plane potential for two vortices at a distance  $R$  by integrating over the radial coordinate from  $\xi$ , the coherence length, to  $R$

$$V_{z,z}(R) \approx -2\varepsilon_0 d \begin{cases} \ln \frac{R}{\xi}, & R \ll \lambda, \\ \ln \frac{\lambda}{\xi} + \left[1 - \frac{\Phi_t(z)}{\Phi_0}\right] \ln \frac{R}{\lambda}, & \lambda \ll R, \end{cases} \quad (9)$$

where  $\Phi_t(z)$  is the magnetic flux trapped by a pancake vortex placed at a distance  $z$  away from the surface. From (8), we find that the trapped flux  $\Phi_t(z)$  interpolates between the values  $(d/\lambda)\Phi_0$  on the surface and  $(d/2\lambda)\Phi_0$  in the bulk,

$$\Phi_t(z) = \frac{\Phi_0 d}{2\lambda} \left(1 + e^{-2z/\lambda}\right). \quad (10)$$

However, we can safely ignore the small modifications of order  $d/\lambda$  in the potential (9) arising from magnetic screening and assume an in-plane interaction which is independent of  $z$ . Within this approximation, vortices in the same layer feel a repulsive logarithmic interaction,

$$V_{z,z}(R) \approx -2\varepsilon_0 d \ln(R/\xi). \quad (11)$$

This potential corresponds to the one between charges in the two-dimensional Coulomb gas, or, equivalently, the one-component plasma (OCP), with charge  $e^2 \rightarrow 2\varepsilon_0 d$ .

### B. Out-of-plane interaction

For two pancake vortices in different layers (cf. Fig. 2(b)), the current (5) which enters the Lorentz force (4) does not contain the contribution from the driving phase  $\nabla\varphi$ . Hence, the force in (5) is due to the vector potential  $\mathbf{A}$  alone. The central quantity in the discussion is the vector field (7) which is produced by a single pancake vortex placed in a semi-infinite sample.

#### SMALL IN-PLANE SEPARATION $R \ll \lambda$

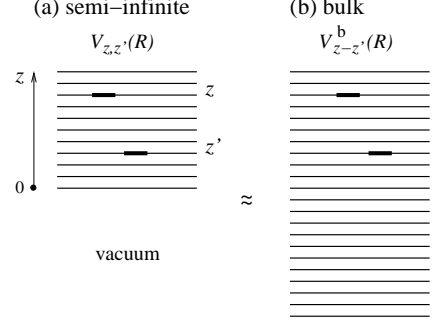


FIG. 3: For small in-plane separation, i.e.,  $R \ll \lambda$ , the total energy for the out-of-plane interaction in a semi-infinite system (a) is equivalent to the one of a translation invariant bulk (b) system  $V_{z-z'}^b(R)$ .

Inserting the vector potential (7) into (4) and (5), we obtain an expression for the force between two pancake vortices residing in different layers  $z \neq z'$ . The integration over  $R$  provides the out-of-plane interaction

$$V_{z,z'}(R) = -\varepsilon_0 d^2 \int_0^{+\infty} dK \frac{J_0(KR)}{KK_+} \times [f_{z-z'}(K) + \beta(K)f_{z+z'}(K)]. \quad (12)$$

This interaction is given by the sum of a bulk- (first)  $V_{z-z'}^b(R)$  and a stray-field term (second)  $V_{z,z'}^s(R)$ , where the latter becomes negligible at a distance  $\sim \lambda$  away from the surface.

For small in-plane distances, i.e.,  $R \ll \lambda$ , the contribution of the stray-field potential to the overall vortex interaction energy can be neglected:  $V_{z,z'}^s(R) \ll V_{z-z'}^b(R)$ . Thus, for  $R \ll \lambda$ , the potential coincides with the bulk one<sup>29</sup>

$$V_{z,z'}(R) \approx \varepsilon_0 d \frac{d}{\lambda} \begin{cases} \frac{R^2}{4|z-z'|\lambda}, & R \ll |z-z'| \ll \lambda, \\ \frac{R}{\lambda}, & |z-z'| \ll R \ll \lambda. \end{cases} \quad (13)$$

As expected, the out-of-plane interaction is smaller with respect to the in-plane expression (11) due to the small pre-factor  $d/\lambda$ . However, the out-of-plane interaction extends over many  $(\lambda/d)$  layers, underlying its importance. In the regime  $R \ll \lambda$ , the attractive interaction between a single pancake vortex and a semi-infinite stack then is reduced close to the surface due to the missing planes for  $z < 0$ .

On the other hand, for large in-plane distances, i.e.,  $R \gg \lambda$ , we find relevant modifications of the out-of-plane interaction at the surface

$$V_{z,z'}(R) \approx \varepsilon_0 d \frac{d}{\lambda} e^{-|z-z'|/\lambda} \ln \frac{R}{\lambda} + \varepsilon_0 d \frac{d}{\lambda} e^{-(z+z')/\lambda} \left( \ln \frac{R}{\lambda} + \frac{2\lambda}{R} \right). \quad (14)$$

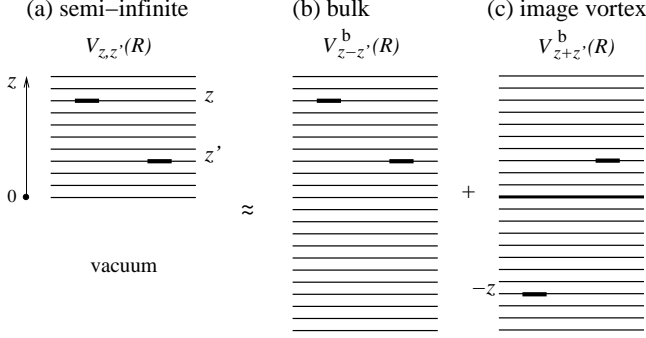
LARGE IN-PLANE SEPARATION  $R \gg \lambda$ 

FIG. 4: For large in-plane separation, i.e.,  $R \gg \lambda$ , the total energy for the out-of-plane interaction in a semi-infinite system (a) can be split in (b) a translation invariant bulk term  $V_{z-z'}^b(R)$  and (c) an additional one  $V_{z+z'}^b(R)$  that can be interpreted in terms of an image vortex placed in  $-z$ . The stray field contributes via an additional algebraic correction, cf. (15)

The first term has a bulk origin, whereas the terms which follow vanish away from the surface. Combining terms, we can rewrite (14) in the more convenient form

$$V_{z,z'}(R) = 2\varepsilon_0 d \left[ \frac{\Phi_t(z, z')}{\Phi_0} \ln \frac{R}{\lambda} + \frac{d}{\lambda} e^{-(z+z')/\lambda} \frac{\lambda}{R} \right]. \quad (15)$$

We identify two different contributions: a logarithmic attractive interaction (first) and an algebraic repulsive potential (second). The logarithmic interaction can be analyzed by considering the presence of mirror vortices in  $z < 0$ . The two terms in  $\Phi_t(z, z')$  can be viewed as the contributions of two bulk vortices, one at  $z$  and a mirror one at  $-z$ , see Fig. 4. Hence, if we consider only the logarithmic term in (15), the interaction between a pancake vortex and a stack in a semi-infinite system is equivalent to that in a bulk system. Modifications appear due to the stray magnetic field, generating the residual algebraic potential in (15). This correction  $\propto \lambda/R$  is responsible for the weak algebraic interaction between vortex tips at large distances<sup>30</sup>.

Summarizing, for short in-plane distances,  $R \ll \lambda$ , the strength of the out-of-plane potential is not affected by the semi-infinite geometry (see Fig. 3) and the effect of the surface is limited to the lack of superconducting planes at  $z < 0$ . On the other hand, for large in-plane distances,  $R \gg \lambda$ , the missing planes are compensated by the contributions from the mirror term in (14), see Fig. 4. Surface effects then are due to the stray magnetic field generating an additional algebraic repulsion, cf. Eq. (15).

### III. DFT-SUBSTRATE APPROACH

Here, we briefly discuss the DFT-substrate approach we will use in our analysis (see Ref. 22 for details). In

the classical DFT one writes the total grand canonical free energy difference from the homogeneous liquid phase as a functional of the (averaged) density profile. In an anisotropic system such as the pancake vortex system, it is convenient to separate the in-plane dependence from the out-of-plane one. Hence, the DFT free energy takes the form

$$\frac{\delta\Omega[\rho_z(\mathbf{R})]}{T} = \int \frac{dz}{d} d^2\mathbf{R} \left[ \rho_z(\mathbf{R}) \ln \frac{\rho_z(\mathbf{R})}{\bar{\rho}} - \delta\rho_z(\mathbf{R}) - \frac{1}{2} \int \frac{dz'}{d} d^2\mathbf{R}' \delta\rho_z(\mathbf{R}) c_{z,z'}(|\mathbf{R}-\mathbf{R}'|) \delta\rho_{z'}(\mathbf{R}') \right], \quad (16)$$

where  $\rho_z(\mathbf{R})$  is the averaged vortex density in the layer  $z$  and  $\delta\rho_z(\mathbf{R}) = \rho_z(\mathbf{R}) - \bar{\rho}$  is the deviation from the homogeneous liquid density  $\bar{\rho}$ . The only input needed in the DFT free energy is the direct correlation function  $c_{z,z'}(R)$ . In our approach we implement the substrate model<sup>9</sup> for the pair-correlation function by separating the contributions of the strong in-plane logarithmic repulsion from the weak out-of-plane but long-range attraction,

$$c_{z,z'}(R) = dc^{2D}(R)\delta(z-z') - V_{z,z'}(R)/T, \quad (17)$$

where  $V_{z,z'}(R)$  is the out-of-plane interaction of Eq. (12); the above approximation for the correlator is described in detail in Ref. 22. Within the planes, vortices are strongly correlated due to the repulsive logarithmic interactions (we neglect small contributions of order  $d/\lambda$  and use (11)). Hence, we can approximate  $c_{z,z}(R)$  with the direct correlation function  $c^{2D}(R)$  of two-dimensional logarithmically interacting particles (also known as one-component plasma, OCP). Instead of using an approximate scheme, such as the hypernetted chain equation<sup>20</sup>, we use results of Monte Carlo simulations of the two-dimensional OCP at various coupling constants  $\Gamma = 2\varepsilon_0 d/T$  to extract  $c^{2D}(R)$ . On the other hand, the out-of-plane direct correlator  $c_{z,z'}(R)$  is determined within perturbation theory<sup>31</sup> in terms of the weak out-of-plane potential; neglecting higher-order correlations, we approximate it with the leading unperturbed value  $-V_{z,z'}(R)/T$ .

At a mean-field level the thermodynamically stable state corresponds to the minimal free energy configuration of the functional (16). Then, the density functions  $\rho_z(R)$  must obey the saddle-point equation

$$\ln \frac{\rho_z(\mathbf{R})}{\bar{\rho}} = \int \frac{dz'}{d} \int d^2\mathbf{R}' c_{z,z'}(|\mathbf{R}-\mathbf{R}'|) \delta\rho_{z'}(\mathbf{R}'). \quad (18)$$

A key quantity in our discussion is the molecular field<sup>19,32,33</sup>  $\xi_z(\mathbf{R})$  defined through

$$\xi_z(\mathbf{R}) = \ln[\rho_z(\mathbf{R})/\bar{\rho}]. \quad (19)$$

Combining the saddle point equation (18) with (19), the molecular field becomes

$$\xi_z(\mathbf{R}) = \int \frac{dz'}{d} \int d^2\mathbf{R}' c_{z,z'}(|\mathbf{R}-\mathbf{R}'|) \delta\rho_{z'}(\mathbf{R}') \quad (20)$$

and represents the average potential produced by the modulated density. However, whereas (19) defines the

molecular field everywhere, Eq. (20) is only valid at the minimum.

Next, instead of seeking the exact form  $\rho_z(\mathbf{R})$  which solves the non-linear integral equations (18), we restrict our analysis to a simple family of periodic functions which describes the modulations of the density in the solid phase. In the following, we concentrate on the simplest case, retaining only the first Fourier components of the density in a triangular lattice,

$$\frac{\rho_z(\mathbf{R})}{\bar{\rho}} = 1 + \sum_{|\mathbf{K}_1|=G} \mu_z e^{i\mathbf{K}_1 \cdot \mathbf{R}} = 1 + \mu_z g(\mathbf{R}), \quad (21)$$

where the vectors  $\mathbf{K}_1$  are the first reciprocal lattice vectors of the frozen structure of length  $G$  which is related to the lattice constant  $a_\Delta$  via  $G = 4\pi/\sqrt{3}a_\Delta$ , and  $\mu_z = \delta\rho_z(G)/\bar{\rho}$  is the Fourier component of the density with wave length  $G$ . In the following discussion, we consider the vortex system as incompressible and neglect the relative density change  $\delta\rho(\mathbf{K} = 0)/\bar{\rho}$ , hence the length of the first reciprocal lattice vectors can be written as  $G = (8\pi^2\bar{\rho}/\sqrt{3})^{1/2}$  (see Ref. 22 for a discussion of how to include the effects of a finite compressibility). The function  $g(\mathbf{R}) = \sum_{|\mathbf{K}_1|=G} e^{i\mathbf{K}_1 \cdot \mathbf{R}} = 2\cos(Gx) + 4\cos(Gx/2)\cos(\sqrt{3}Gy/2)$  includes the sum over the six first reciprocal lattice vectors. We also write a similar Ansatz for the molecular field

$$\xi_z(\mathbf{R}) = \zeta_z + \xi_z g(\mathbf{R}), \quad (22)$$

retaining only the zeroth and first Fourier components,  $\zeta_z$  and  $\xi_z$  respectively. The Fourier components of  $\rho(\mathbf{R})$  and  $\xi(\mathbf{R})$  are not independent and can be related through (19). Filtering out the zeroth and first Fourier components of  $\rho_z(\mathbf{R}) = \bar{\rho}(1 + \mu_z g(\mathbf{R})) = \bar{\rho}\exp(\zeta_z + \xi_z g_{K_1}(\mathbf{R}))$  and using

$$\frac{1}{a} \int_a d^2\mathbf{R} g(\mathbf{R}) = 0, \quad \frac{1}{a} \int_a d^2\mathbf{R} [g(\mathbf{R})]^2 = 6, \quad (23)$$

we obtain the dependencies

$$\zeta_z = -\Phi(\xi_z), \quad \mu_z = \Phi'(\xi_z)/6, \quad (24)$$

where we have defined the function

$$\Phi(\xi) = \ln \left[ \frac{1}{a} \int_a d^2\mathbf{R} e^{\xi g(\mathbf{R})} \right]. \quad (25)$$

Inserting the above Ansatz for the order-parameter profile  $\delta\rho$  into the free energy (16), we obtain the associated free energy density functional ( $A$  is the sample area)  $\delta\omega/T = (1/\bar{\rho}A)\delta\Omega/T$  expressed through  $\mu_z$

$$\frac{\delta\omega[\mu_z]}{T} = \int_0^\infty \frac{dz}{d} \left[ 6\xi_z \mu_z - \Phi(\xi_z) - 3 \int_0^\infty \frac{dz'}{d} \bar{c}_{z,z'} \mu_{z'} \mu_z \right], \quad (26)$$

where

$$\bar{c}_{z,z'} = \bar{c}^{2D} \delta(z - z') - V_{z,z'}(G)/T \quad (27)$$

is the dimensionless Fourier transform<sup>34</sup> of the direct correlation function  $\bar{c}_{z,z'} = c_{z,z'}(G)$  evaluated at the first reciprocal lattice vector  $G$ . Consistently, we have defined  $\bar{c}^{2D} = c^{2D}(G)$ . The effects of stray fields are accounted for within the out-of-plane interaction  $V_{z,z'}(G)$  of Eq. (12),

$$\begin{aligned} \frac{V_{z,z'}(G)}{T} &= -\frac{2\pi\bar{\rho}\Gamma d}{G^2\lambda^2 G_+} \left( e^{-G_+|z-z'|} + \frac{G_+ - G}{G_+ + G} e^{-G_+(z+z')} \right) \\ &= -\bar{\alpha}(\bar{f}_{z-z'} + \bar{\beta}\bar{f}_{z+z'}). \end{aligned} \quad (28)$$

In (28) we have defined  $\bar{f}_z = f_z(G) = \exp(-G_+|z|)$ ,  $\bar{\alpha} = \alpha(G) = 2\pi\bar{\rho}\Gamma d/G^2\lambda^2 G_+$ ,  $\bar{\beta} = (G_+ - G)/(G_+ + G)$ , and  $G_+ = \sqrt{G^2 + 1/\lambda^2}$ . Note the additional factor  $\bar{\rho}$  due to the dimensionless definition of the Fourier transform. Combining (26) with (27) and (28) and after few simple algebraic manipulations we obtain the functional

$$\begin{aligned} \frac{\delta\omega[\mu_z]}{T} &= \int_0^\infty \frac{dz}{d} \left[ \frac{\delta\omega_{\text{sub}}^{2D}(\mu_z)}{T} \right. \\ &\quad + \frac{3\bar{\alpha}}{2} \int_0^\infty \frac{dz'}{d} (\bar{f}_{z-z'} + \bar{f}_{z+z'}) (\mu_z - \mu_{z'})^2 \Big] \\ &\quad + \frac{6\bar{\alpha}G}{G + G_+} \int_0^\infty \frac{dz}{d} \int_0^\infty \frac{dz'}{d} \bar{f}_{z+z'} \mu_z \mu_{z'}. \end{aligned} \quad (29)$$

The first term in (29) describes the local two-dimensional free energy of a uniform system

$$\delta\omega_{\text{sub}}^{2D}(\mu)/T = 6\xi(\mu)\mu - \Phi(\xi(\mu)) - 3\bar{c}_{\text{sub}}^{2D}\mu^2, \quad (30)$$

where  $\xi$  has to be understood as a function of  $\mu$  through (24). In (30) we have defined the correlator

$$\bar{c}_{\text{sub}}^{2D} = \bar{c}^{2D} - V_{\text{stack}}(G)/T, \quad (31)$$

where the out-of-plane interactions contribute to the correlator through the total stack potential

$$-\frac{V_{\text{stack}}(G)}{T} = -\bar{\alpha} \int_0^{+\infty} \frac{dz}{d} (\bar{f}_{z-z'} + \bar{f}_{z+z'}) = \frac{2\bar{\alpha}}{dG_+}. \quad (32)$$

The additional non-local terms in (29) quantify the energy cost due to variations of the order parameter (the non-local ‘elastic’ term, second line) and the effect of the surface (third line).

The free-energy (29) has to be compared with the phenomenological Landau-type functional of Eq. (1). Both expressions exhibit a similar structure composed by a sum of bulk, ‘elastic’, and surface terms. However, the analysis of the free energy (29) is complicated by the non-local nature of the ‘elastic’ and surface terms.

#### IV. BULK SYSTEM

Before concentrating on the surface problem, we briefly review the case of an infinite bulk system. The results in this section will be the basis for the discussion of the melting transition in the semi-infinite geometry which we will present in the following sections.

In a bulk system, we can drop the surface term and the free energy (29) becomes

$$\frac{\delta\omega[\mu_z]}{T} = \int_{-\infty}^{\infty} \frac{dz}{d} \left[ \frac{\delta\omega_{\text{sub}}^{2D}(\mu_z)}{T} + \frac{3\bar{\alpha}}{2} \int_{-\infty}^{\infty} \frac{dz'}{d} \bar{f}_{z-z'} (\mu_{z'} - \mu_z)^2 \right]. \quad (33)$$

Below, we first concentrate on the thermodynamically stable state (see also Ref. 22) and then analyze the properties of a solid-liquid interface.

### A. Thermodynamic phase diagram

In thermodynamic equilibrium, all superconducting layers are equivalent and the order parameter  $\mu_z$  becomes independent of the layer position  $z$ , hence we write  $\mu_z = \mu$ . For a constant order-parameter profile the second term in (33) is zero and only the bulk free energy of Eq. (30) is relevant. The key quantity is the effective three-dimensional correlator  $\bar{c}_{\text{sub}}^{2D}$  which is given by the sum of two contributions: the OCP term  $\bar{c}^{2D}$  and the stack potential  $V_{\text{stack}}(G)$  of Eq. (32). Whereas the first depends only on the temperature, the latter depends also on the vortex density and thus on the magnetic field,

$$\begin{aligned} \bar{c}_{\text{sub}}^{2D}(T, B) &= \bar{c}^{2D}(T) + \frac{4\pi\bar{\rho}\varepsilon_0 d}{TG^2} \frac{1}{1 + \lambda^2 G^2} \\ &= \bar{c}^{2D}(T) + \frac{\sqrt{3}\varepsilon_0 d}{2\pi T} \frac{1}{[1 + (8\pi^2/\sqrt{3})B/B_\lambda]}, \end{aligned} \quad (34)$$

where we use  $\bar{\rho}/G^2 = \sqrt{3}/(8\pi^2)$  and  $\lambda^2 G^2 = (8\pi^2/\sqrt{3})B/B_\lambda$ , with  $B_\lambda = \Phi_0/\lambda^2$ .

The temperature and magnetic field dependencies entering  $\bar{c}_{\text{sub}}^{2D}(T, B)$  change the coefficient of the quadratic term as in the  $\phi^4$  Landau theory. As a function of  $\mu$ , the free energy exhibits the shape of a Landau theory describing a first-order phase transition (this function is plotted in Ref. 22): for small values of the correlator  $\bar{c}_{\text{sub}}^{2D}$ , corresponding to large temperatures and fields,  $\delta\omega^{2D}(\mu)$  exhibits only one minimum at  $\mu_1 = 0$  with a value  $\delta\omega^{2D}(0)/T = 0$ , corresponding to a (homogeneous) liquid phase. Decreasing the temperature and/or field (which corresponds to increasing values of  $\bar{c}_{\text{sub}}^{2D}$ ), a second local minimum at  $\mu_s > 0$  (metastable solid) appears in addition to the liquid one at  $\mu_1 = 0$ . Freezing occurs when the liquid and solid minima assume the same value of the free energy, i.e., when  $\delta\omega^{2D}(\mu_s) = 0$ . This condition is equivalent to a simple equation for the correlator<sup>32</sup>

$$\bar{c}_{\text{sub}}^{2D}(T, B) = \bar{c}_c \approx 0.856. \quad (35)$$

Solving this equation for  $B$  yields the melting line, see Ref. 22. Going to even lower temperatures,  $\bar{c}^{2D}$  further increases, the solid minimum decreases further,  $\delta\omega^{2D}(\mu_s)/T < 0$ , and the crystal becomes the only thermodynamically stable phase.

### B. Solid-liquid interface

Next, we consider a solid-liquid interface in an infinite system, for which both terms in (33) are important. Along the melting line  $B_m(T)$  the solid and the liquid assume the same value of the free energy and can coexist. Here, we analyze the situation where half of the system is in the liquid state and the other half is solid. The corresponding profile of  $\mu_z$  takes the form of a soliton with boundary conditions  $\mu_{z \rightarrow -\infty} = 0$  (liquid) and  $\mu_{z \rightarrow +\infty} = \mu_s \approx 0.51$  (solid), where  $\delta\omega_{\text{sub}}^{2D}(0)/T = \delta\omega_{\text{sub}}^{2D}(\mu_s)/T = 0$ . The properties of the interface between the two phases depend on the non-local term in the free-energy functional (33). For a large part of the phase diagram (see Appendix A), it is possible to approximate the full non-local theory with a local one by proceeding with a gradient expansion<sup>35,36</sup> of the kernel in (33); inserting  $\mu_{z'} \approx \mu_z + (d\mu_z/dz)(z' - z)$  into (33), we obtain

$$\frac{\delta\omega[\mu_z]}{T} = \int_{-\infty}^{\infty} \frac{dz}{d} \left[ \frac{\delta\omega_{\text{sub}}^{2D}(\mu_z)}{T} + \frac{\ell^2}{2} \left( \frac{d\mu_z}{dz} \right)^2 \right], \quad (36)$$

with the elastic scale

$$\begin{aligned} \ell^2 &= \frac{3\bar{\alpha}}{d} \int_{-\infty}^{+\infty} dz \bar{f}_{zz} z^2 = \frac{12\bar{\alpha}}{dG_+^3} = \\ &= \lambda^2 \frac{3\sqrt{3}}{2\pi} \frac{\Gamma}{[1 + (8\pi^2/\sqrt{3})B_m(T)/B_\lambda]^2}. \end{aligned} \quad (37)$$

This local approximation describes well the full non-local free energy if the profile  $\mu_z$  varies slowly over the extension  $1/G_+$  of the kernel. We have checked that this condition is fulfilled for  $T \gtrsim 0.04\varepsilon_0 d$ , which corresponds to small and moderate magnetic fields  $B \lesssim 0.5B_\lambda$ , by comparing the shape of the soliton in the non-local and local theories (see Appendix A).

We can easily estimate the main properties of the solid-liquid interface, e.g. its width and free energy cost. At small magnetic fields, we use the gradient expansion and write the Euler-Lagrange equation of the free-energy functional (36)

$$\ell^2 \frac{d^2 \mu_z}{dz^2} = \frac{d}{d\mu_z} \left( \frac{\delta\omega_{\text{sub}}^{2D}(\mu_z)}{T} \right) \quad (38)$$

and the corresponding energy conservation (the integration constant is zero for a soliton solution)

$$\frac{d\mu_z}{dz} = \frac{1}{\ell} \sqrt{\frac{2\delta\omega_{\text{sub}}^{2D}(\mu_z)}{T}}. \quad (39)$$

The energy  $E_{\text{sl}}$  of the interface (soliton) is given by

$$\begin{aligned} E_{\text{sl}} &= T \int \frac{dz}{d} \ell^2 \left( \frac{d\mu_z}{dz} \right)^2 = T \frac{\ell}{d} \int_0^{\mu_s} d\mu \sqrt{\frac{2\delta\omega_{\text{sub}}^{2D}(\mu)}{T}} \\ &= CT \frac{\ell}{d} \mu_s \sqrt{\frac{2\delta\omega_{\text{max}}^{2D}}{T}}, \end{aligned} \quad (40)$$

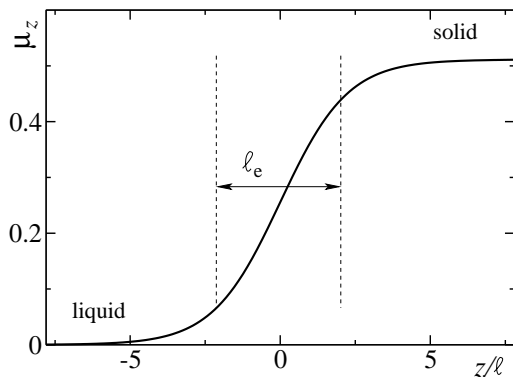


FIG. 5: Profile of the order parameter  $\mu_z$  describing an interface between a liquid ( $\mu_{z \rightarrow -\infty} = \mu_l = 0$ ) and a solid ( $\mu_{z \rightarrow +\infty} = \mu_s \approx 0.51$ ). The shape has been obtained numerically by solving the differential equation (38). The width of the interface is approximately  $\ell_e \approx 4.05 \ell$  (we define it as the full width at half maximum of the function  $d\mu_z/dz$ ), where  $\ell$  is defined in (37).

where  $\delta\omega_{\max}^{2D} \approx 0.0065 T$  is the barrier in the energy density between the solid and liquid minima on the melting line and  $\mu_s \approx 0.51$ . The constant  $C$  is of order unity and requires to evaluate the integral in (40): a numerical calculation gives  $C \approx 0.69$ .

Next, we determine the width of the soliton  $\ell_e$ , which we define as the full width at half maximum of the derivative  $d\mu_z/dz$ . Approximating  $d\mu_z/dz \approx \mu_s/\ell_e$  in (40), we obtain an estimate for the soliton energy  $E_{sl} \approx T\ell^2(\ell_e/d)(\mu_s/\ell_e)^2$ . Combining this formula together with (40), we find

$$\ell_e \approx \frac{\mu_s}{\sqrt{2\delta\omega_{\max}^{2D}/T}} \ell. \quad (41)$$

From (41), we obtain  $\ell_e \approx 6.33 \ell$ ; however, a precise determination of the proportionality factor requires a numerical study, which yields  $\ell_e \approx 4.05 \ell$ , see Fig. 5. At low fields,  $B \rightarrow 0$  (and  $T \rightarrow T_{\text{BKT}}$ ), the soliton becomes wider than the bulk penetration depth,  $\ell_e \approx 8\lambda$ , see (41) and (37). This confirms the validity of the gradient expansion for  $B \rightarrow 0$ , since in this limit  $1/G_+ \approx \lambda$  and  $\ell_e G_+ \approx 8$ .

On the other hand, for large  $B$ , the gradient expansion is not valid and we cannot use Eq. (41). However, we have determined numerically the shape of the soliton (see Appendix A) using the full non-local theory (33) and found its width to decrease with increasing  $B$  (the full theory produces a sharper interface than the one originating from the gradient approximation). We can interpret this results in terms of the intra-layer interactions dominating over the inter-layer ones, leading to a system of decoupled 2D planes which melt independently.

## V. SURFACE MELTING

The presence of a surface modifies the bulk free energy functional (33) in two ways as it is clear from (29): *i*) the

superconductor occupies only a half-infinite space  $z > 0$ , *ii*) stray magnetic fields modify the vortex interaction and hence the direct correlation function  $\bar{c}_{z,z'}$  near the surface.

The configuration of the system is derived from the saddle-point equation of (29). Minimization with respect to  $\mu_z$  provides us with the integral equation

$$\begin{aligned} \frac{\partial_{\mu_z} \delta\omega_{\text{sub}}^{2D}(\mu_z)}{T} + 6\bar{\alpha} \int_0^\infty \frac{dz'}{d} [\bar{f}_{z-z'} + \bar{f}_{z+z'}](\mu_z - \mu_{z'}) \\ + \frac{12\bar{\alpha}G}{G_+ + G_+} \int_0^\infty \frac{dz'}{d} \bar{f}_{z+z'} \mu_{z'} = 0. \end{aligned} \quad (42)$$

The surface produces two additional terms when compared to an infinite system: a mirror term ( $\propto \bar{f}_{z+z'}$ ) in the non-local elastic force and a pure surface term (second line), cf. the discussion of the out-of-plane interaction in Sec. II B.

In the following, we first acquaint ourselves with the formalism by studying the  $B \approx 0$  and large field limits. Then, we present the full analysis at low but finite values of the magnetic field.

### A. Large magnetic field and $B \approx 0$ limits

Let us consider first large magnetic fields,  $B \gg B_\lambda$ . In this limit, the contribution of the out-of-plane potential vanishes ( $G \approx (B/\Phi_0)^{1/2} \rightarrow \infty$  and  $\bar{\alpha} \rightarrow 0$ ) and the system decouples into independent two-dimensional systems. Only the intra-layer interaction remains relevant in this limit and the free energy is simply given by the bulk local contribution (30). The saddle point equation

$$\partial_{\mu_z} \delta\omega_{\text{sub}}^{2D}(\mu_z)/T = 0 \quad (43)$$

does not depend on  $z$  and the solution is given by a constant order parameter profile. Thus, no modifications occur at the surface for  $B \gg B_\lambda$ .

In the opposite limit of  $B \rightarrow 0$  ( $G \rightarrow 0$ ),  $G_+ \approx 1/\lambda$  and  $\bar{\alpha}$  remain finite. The surface term in (29) is negligible and the saddle point equation

$$\frac{\partial_{\mu_z} \delta\omega_{\text{sub}}^{2D}(\mu_z)}{T} + 6\bar{\alpha} \int_0^\infty \frac{dz'}{d} [\bar{f}_{z-z'} + \bar{f}_{z+z'}](\mu_z - \mu_{z'}) = 0,$$

contains an additional term as compared to (43). However, we can render the problem translational invariant on the whole  $z$ -axis, by introducing mirror vortices in  $z < 0$  via  $\mu_{-z} = \mu_z$  and changing  $z' \rightarrow -z'$  in the integral of the mirror term. As a result, we can map the semi-infinite system back to the infinite bulk and the constant bulk solution remains valid also in this limit. We can conclude that for both  $B \approx 0$  and  $B \gg B_\lambda$  the surface does not lead to a modification of the bulk behavior.

### B. Low magnetic fields

At finite magnetic fields, all three terms of the saddle-point equation (42) are relevant. To understand the effect



of the surface term (third), it is convenient to look at the associated free energy expression (cf. (29)), which can be written as a weighted square of  $\mu_z$ ,

$$\frac{\delta\omega^s[\mu_z]}{T} = \frac{6\bar{\alpha}G}{G+G_+} \left( \int_0^\infty \frac{dz}{d} e^{-G_+z} \mu_z \right)^2. \quad (44)$$

This term favors the appearance of the liquid on the surface, similarly to the local surface term in (1). In real space, (44) is associated with the  $\propto 1/R$  repulsive potential induced by the stray magnetic field, cf. the second term in (15). In analogy to the Landau-theory description of Eq. (1), this DFT functional can yield two different surface melting scenarios: discontinuous,  $O_1$ , and continuous,  $O_2$  (see introduction).

To make progress analytically, we have to simplify the non-local terms in (42). Concentrating on the bulk, i.e.,  $z \gg 1/G_+$ , both mirror and surface terms can be ignored. For not too large values of the magnetic fields, we can adopt a gradient expansion of the non-local elastic term  $\propto \bar{f}_{z-z'}$ , cf. Sec. IV B and Appendix A. As a result we obtain the differential equation

$$\ell^2 \frac{d^2 \mu_z}{dz^2} = \frac{d}{d\mu_z} \frac{\delta\omega_{\text{sub}}^{2D}(\mu_z)}{T} \quad (45)$$

with  $\ell^2 = (6\bar{\alpha}/d) \int_0^\infty dz \bar{f}_z z^2 = 12\bar{\alpha}/dG_+^3$ , cf. Eq. (37). Equation (45) has to be completed with a boundary condition, which has to be provided by the surface term in the integral equation. In the following, we restrict the analysis to small values of the order parameter at the surface in order to study the boundary between continuous and discontinuous surface melting scenarios. In this regime the bulk potential (30) can be approximated as

$$\delta\omega_{\text{sub}}^{2D}(\mu)/T \approx 3(1 - \bar{c}_c)\mu^2, \quad (46)$$

where we used  $\Phi(\xi) \approx 3\xi^2$  (cf. (25)),  $\mu = \Phi'(\xi)/6 \approx \xi$  (using (24) together with (23)) and the value of the critical correlator  $\bar{c}_{\text{sub}}^{2D} = \bar{c}_c \approx 0.856$  at melting. The saddle point equation takes the form of a linear integral equation

$$6(1 - \bar{c}_c)\mu_z + 6\bar{\alpha} \int_0^\infty \frac{dz'}{d} [\bar{f}_{z-z'} + \bar{f}_{z+z'}](\mu_z - \mu_{z'}) + \frac{12\bar{\alpha}G}{G+G_+} \int_0^\infty \frac{dz'}{d} \bar{f}_{z+z'} \mu_{z'} = 0 \quad (47)$$

with three terms: a potential force (first), a non-local elastic force (second) and the drive at the surface (third). Separating the non-local terms from the local ones, we obtain

$$\left[ 6(1 - \bar{c}_c) + \frac{12\bar{\alpha}}{dG_+} \right] \mu_z = 6\bar{\alpha} \int_0^\infty \frac{dz'}{d} [\bar{f}_{z-z'} + \bar{\beta} \bar{f}_{z+z'}] \mu_{z'}, \quad (48)$$

where  $\bar{\beta}$  was defined in (28). The second term in the left hand side carries the normalization of the kernel  $\bar{f}_z$  (from the integral  $6\bar{\alpha} \int_0^\infty (dz'/d) [\bar{f}_{z-z'} + \bar{f}_{z+z'}] = 12\bar{\alpha}/G_+d$  in

the elastic term of (47)). Equation (48) can be rewritten as

$$\mu_z = \frac{G_+}{2(1+r)} \int_0^\infty dz' [\bar{f}_{z-z'} + \bar{\beta} \bar{f}_{z+z'}] \mu_{z'}, \quad (49)$$

with  $r = dG_+(1 - \bar{c}_c)/2\bar{\alpha} = 6(1 - \bar{c}_c)/(G_+\ell)^2$ .

This kind of integral equation is commonly found in the study of boundary problems, e.g. in the analysis of surface effects on the superconducting transition<sup>38,39</sup>. For the latter case, the equation which determines the superconducting gap  $\Delta(r)$  is a non-local integral equation with a structure similar to (48) (or (49)). Close to the superconducting transition  $T_c$ , a gradient expansion reduces the non-local equation into the local Ginzburg-Landau equation. The presence of the surface enters the kernel of the non-local theory via an additional contribution, corresponding to the term  $\propto \bar{f}_{z+z'}$  in (48). However, a major difference between the two problems is given by the different nature of the bulk phase transitions, first order for the melting and second order for the superconducting transition. In the case of a second-order phase transition the coefficient of the quadratic term in the bulk free energy goes to zero at the transition point, cf. the coefficient  $\alpha \sim (T - T_c)$  in the Ginzburg-Landau equation. Hence, the term corresponding to the force  $\propto 6(1 - \bar{c}_c)$  in the LHS of (48) is absent. In Eq. (49) the difference between a first- and a second-order bulk transition enters in the normalization of the integral in the RHS, through the parameter  $r$ , which is  $r \neq 0$  for a first-order transition and  $r = 0$  for a second-order one.

In general, the solution of an integral equation of the type (49) is a non-trivial task, which usually cannot be carried out exactly. However, in the present case a straightforward solution is possible due to the particular exponential form of the kernel. In fact, taking the second derivative of (49) and making use of the identity

$$\frac{d^2}{dz^2} e^{-G_+|z-z'|} = -2G_+ \delta(z-z') + G_+^2 e^{-G_+|z-z'|}, \quad (50)$$

we find that the integral equation yields the *same* differential equation (45) as derived previously in the bulk by means of a gradient expansion,

$$(1+r)\ell^2 \frac{d^2 \mu_z}{dz^2} \approx \ell^2 \frac{d^2 \mu_z}{dz^2} = r(\ell G_+)^2 \mu_z = 6(1 - \bar{c}_c)\mu_z; \quad (51)$$

here, we have used the linearized force  $\partial_\mu \delta\omega_{\text{sub}}^{2D}(\mu)/T = 6(1 - \bar{c}_c)\mu_z$  and we can drop the small renormalization factor  $(1+r) \approx 1$  in the LHS of the equation<sup>37</sup>. The differential equation (51) admits two *exponential* solutions. This has to be compared to the case of a second-order bulk transition, where, due to the absence of a linear term in the bulk free energy, one obtains the differential equation  $d^2 \mu_z/dz^2 = 0$  which is solved by a *linear* function<sup>38</sup>. In both cases, the integral equation (49) is equivalent to the *bulk* differential equation (51) and the bulk solution goes through the surface region. Hence,

the effect of the surface terms  $\propto \bar{\beta}$  is only to provide a boundary condition at  $z = 0$  but does not modify the bulk solution. This lucky coincidence is due to the particular exponential structure of the kernel. Usually, the bulk solution is not valid in the vicinity of the surface and the problem becomes much more difficult to solve.

Next, we derive the boundary condition which is provided by the surface term. We first write the general solutions of the bulk differential equation

$$\mu_z = Ae^{\gamma G+z} + Be^{-\gamma G+z}, \quad (52)$$

where  $\gamma^2 = r/(1+r)$ ; the boundary condition then follows from the ratio  $A/B$ . Here, we retain the small correction  $(1+r)$  in (51) as we base our analysis on the linearized integral equation (dropping this term leads to results which are correct to order  $r$ , in agreement with the precision of the gradient expansion). Inserting this Ansatz back into (49), we obtain the condition

$$A\left(\frac{\bar{\beta}}{1-\gamma} - \frac{1}{1+\gamma}\right) + B\left(\frac{\bar{\beta}}{1+\gamma} - \frac{1}{1-\gamma}\right) = 0.$$

This requirement selects a unique value of the ratio  $B/A$ ,

$$\frac{B}{A} = \frac{\gamma(\bar{\beta}+1) + (\bar{\beta}-1)}{\gamma(\bar{\beta}+1) - (\bar{\beta}-1)}. \quad (53)$$

Finally, we can calculate the logarithmic derivative at  $z = 0$ , which gives the relevant boundary condition for our forthcoming analysis, cf. Eq. (3), and we find the result (we define  $\mu'_z = \partial_z \mu_z$ )

$$\frac{\mu'_z}{\mu_z}\Big|_{z=0} = G_+ \gamma \frac{A-B}{A+B} = G_+ \frac{1-\bar{\beta}}{1+\bar{\beta}} = G. \quad (54)$$

This final relation can also be derived directly without solving the differential equation at the surface: calculating the value of the order parameter and its derivative at  $z = 0$  from (49), one finds

$$\mu_0 = \frac{G_+}{2(1+r)}(1+\bar{\beta}) \int_0^\infty dz \bar{f}_z \mu_z, \\ \frac{d\mu_z}{dz}\Big|_{z=0} = \frac{G_+}{2(1+r)} G_+(1-\bar{\beta}) \int_0^\infty dz \bar{f}_z \mu_z.$$

The ratio  $\mu'_0/\mu_0$  then does not depend on the function  $\mu_z$  which has dropped out. As a result we recover (54), which also remains valid for the case of a bulk second-order phase transition ( $r = 0$ ). In the limit  $B \approx 0$ , the boundary condition becomes  $\mu'_0 = 0$ , since  $G \approx 0$ . Hence, the constant bulk solution goes through and the surface is not relevant, in agreement with the results of Sec. V A.

The analysis of the boundary value problem (45) with (54) follows the one in Ref. 18. Combining the expression for the ‘conserved energy’ (originating from the bulk equation (45))

$$\ell \mu'_z = \sqrt{\frac{2\delta\omega_{\text{sub}}^{2D}(\mu_z)}{T}} \quad (55)$$

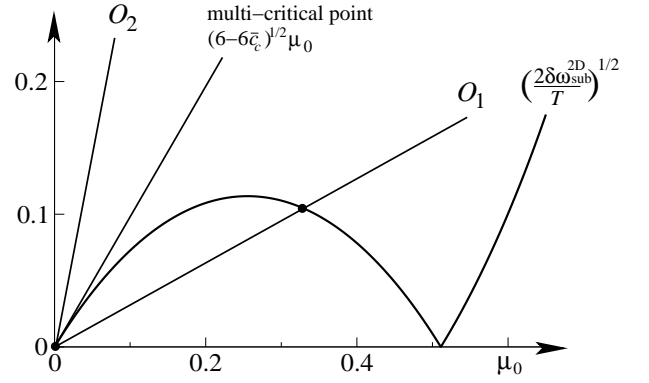


FIG. 6: Graphical solution of (56) for  $\mu_0$ . We plot separately the RHS of (56),  $\sqrt{2\delta\omega_{\text{sub}}^{2D}(\mu_0)/T}$ , and the LHS,  $\ell G\mu_0$ , for different values of the slope  $\ell G$ . For  $\ell G < \sqrt{6(1-\bar{c}_c)}$  we find an intersection point at a  $\mu_0 > 0$  (besides the solution  $\mu_0 = 0$ ). This finite value is the residual order parameter on the surface for the  $O_1$  scenario (surface non-melting). For  $\ell G = \sqrt{6(1-\bar{c}_c)}$  the straight line is tangent to  $\sqrt{2\delta\omega_{\text{sub}}^{2D}(\mu_0)/T}$  at  $\mu_0 = 0$ , the finite solution has disappeared, and only  $\mu_0 = 0$  remains (multi-critical point). For  $\ell G > \sqrt{6(1-\bar{c}_c)}$  the only solution is at  $\mu_0 = 0$  ( $O_2$  scenario, surface melting).

with the boundary condition (54), we find an algebraic relation which determines the value of the order parameter  $\mu_0$  at the surface,

$$\mu_0 \ell G = \sqrt{\frac{2\delta\omega_{\text{sub}}^{2D}(\mu_0)}{T}}. \quad (56)$$

The liquid surface  $\mu_0 = \mu_1 = 0$  is always a solution and we deal with a continuous surface melting ( $O_2$  scenario) if it is the only one. Once a second solution with  $\mu_0 > 0$  is present, the surface undergoes a discontinuous ( $O_1$ ) transition, see Fig. 6. Using the full expression for the potential on the RHS of (56), we find that (56) admits two solutions for large  $T$  (small fields  $B$ ) and only the  $\mu_0 = 0$  solution for small temperatures (large magnetic fields), cf. the solid line in Fig. 7. Since both the continuous and the discontinuous melting scenarios are present, a multi-critical point separating the two different kinds of transitions must exist. The equation which locates the critical point derives from (56) by considering the quadratic expansion of the potential  $\delta\omega_{\text{sub}}^{2D}(\mu)/T \approx 3(1-\bar{c}_c)\mu^2$  (cf. Fig. 6)

$$\frac{\ell(T_{\text{mc}}, B_{\text{mc}})G(B_{\text{mc}})}{\sqrt{6(1-\bar{c}_c)}} = 1 \\ \longrightarrow (T_{\text{mc}}, B_{\text{mc}}) \approx (0.29 \varepsilon_0 d, 0.007 B_\lambda). \quad (57)$$

For  $T < T_{\text{mc}}$  the surface undergoes a continuous transition and acts as a nucleus for the liquid phase, preventing the appearance of the solid metastable phase. On the other hand, for large temperatures  $T > T_{\text{mc}}$  the order parameter at  $z = 0$  still undergoes a residual jump and the double-sided hysteretic behavior is restored, see Figs. 10 and 11.

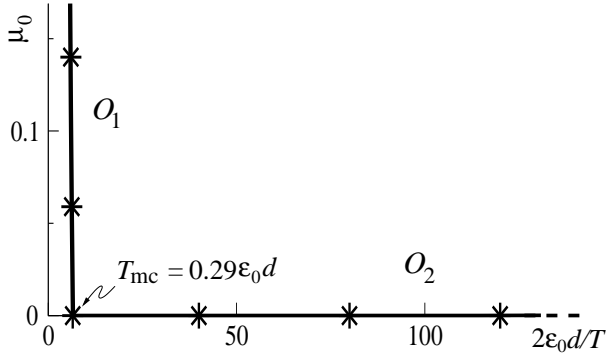


FIG. 7: Residual value of the order parameter at the surface: analytic (solid line) from (56) and full numerical solution (stars) see Section VI. For  $T < T_{mc}$  the surface undergoes a continuous transition ( $O_2$ ), whereas for  $T > T_{mc}$  the order parameter at  $z = 0$  still exhibits a residual jump at melting.

### 1. Multi-critical point at high-fields

At high magnetic fields the layers melt independently following a first-order type 2D-melting scenario. The order parameter  $\mu_0$  in the topmost layer then undergoes a finite jump and the surface non-melting ( $O_1$ ) scenario applies. The presence of a discontinuous  $O_1$  regime at high fields implies the existence of a second multi-critical point. While our analytical approach is not applicable anymore, since it is based on the gradient expansion which is not justified in this regime, numerically we have found clear indications of a finite jump at high fields ( $B \approx 10 B_\lambda$ ). However, a more elaborate version of the DFT is required for an accurate determination of this multi-critical point. In particular, approaching the melting temperature of each 2D lattice, the higher-order peaks in the OCP correlation function  $c^{2D}(K)$  become important ( $K_n > G$ ). Hence, higher components in the Fourier expansion of the density have to be retained<sup>40</sup>, in order to obtain a more precise description of the high-field regime.

### C. Analysis of the continuous surface melting and of the multi-critical point

The fact that a discontinuous bulk transition may turn continuous at the surface is somewhat non-trivial. To obtain a better insight into the mechanism of the continuous surface melting, we present here an alternative analysis. We describe the surface-melting process in the language of the entry of the liquid through the boundary. The appearance of a liquid layer at the surface, while the bulk remains solid, implies the existence of an interface between the two phases, which is described by a soliton-like profile of the order parameter. The entry of the liquid can happen in two different ways: *i*) the soliton can slide smoothly from the boundary at  $T_m$  (surface melting,  $O_2$ ) or *ii*) it starts entering the system but remains pinned

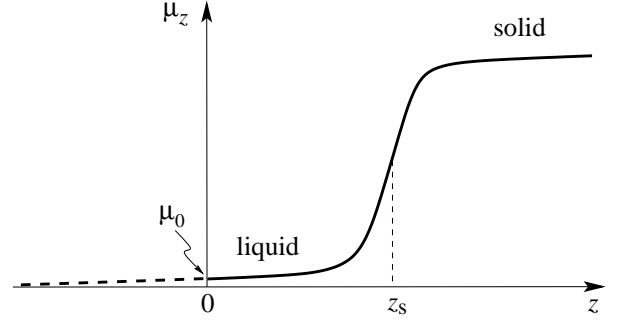


FIG. 8: Sketch of a solid-liquid interface placed at a distance  $z_s$  away from the surface. The surface destabilizing term  $E_{\text{surf}}(z_s)$  of Eq. (60) favors the entry of the liquid-solid interface at the surface, producing a repulsive surface potential on the soliton. On the other hand, the energy cost to push the soliton into the system generates an attractive surface potential  $E_{\text{sl}}(z_s)$ , cf. (61). Depending on which term is dominant, either a continuous or a discontinuous surface melting transition is realized.

near the surface at  $T_m$  (surface non-melting,  $O_1$ ). To distinguish these two scenarios we need to calculate the energy of the soliton as a function of its (half-height) position  $z_s$  away from the surface and the resulting pinning energy. We do this within the local theory described by the functional

$$\frac{\delta\omega}{T} = \int \frac{dz}{d} \left[ \frac{\delta\omega_{\text{sub}}^{2D}(\mu_z)}{T} + \frac{\ell^2}{2} \left( \frac{d\mu_z}{dz} \right)^2 + \frac{\ell^2 G}{2} \mu_z^2 \delta(z) \right]. \quad (58)$$

The saddle point equation of (58) reproduces the equation of state (45) with the boundary condition (54) at  $z = 0$  (cf. Eqs. (2) and (3)).

As in the previous section, we concentrate on the case when the order parameter at the surface is small. Since the bulk solution remains valid also in the vicinity of the surface, we can study the problem within a variational scheme, taking the bulk soliton  $\mu_z^{\text{sl}}(z_s)$  as a convenient variational function and displacing it rigidly at different distances  $z_s$  from the surface ('sl' stands for solid-liquid interface), see Fig. 8.

We proceed with the estimate of the energy due to a solid-liquid interface at  $z_s$ , which is given by  $\delta\omega[\mu_z^{\text{sl}}(z_s)]$ . In the following, we want to calculate the soliton energy not only at the bulk transition temperature  $T_m$  but also at temperatures  $T$  close by. However, for  $T \neq T_m$ , the free energy  $\delta\omega[\mu_z^{\text{sl}}(z_s)]$  is infinite due to the contribution from the bulk solid  $\delta\omega_{\text{sub}}^{2D}(\mu_s) \neq 0$ . In order to obtain a finite energy, which correctly estimates the soliton energy  $E_{\text{sl}}^{\text{surf}}(z_s)$  in the presence of the surface we have to subtract this infinite contribution. We therefore define

$$E_{\text{sl}}^{\text{surf}}(z_s) \equiv \delta\omega[\mu_z^{\text{sl}}(z_s)] - (L/d)\delta\omega_{\text{sub}}^{2D}(\mu_s, T) \quad (59)$$

where  $L \rightarrow \infty$  is thickness of the sample. Inserting the function  $\mu_z^{\text{sl}}(z_s)$  in (58), the third term is simple to calculate and yields the surface energy

$$E_{\text{surf}}(z_s) = T \frac{\ell^2 G}{d} \frac{[\mu_0^{\text{sl}}(z_s)]^2}{2}. \quad (60)$$

The first two terms in (58) give the energy of the soliton in the semi-infinite system. For  $T < T_m$ , the presence of a liquid layer of thickness  $\sim z_s$  produces a contribution linear in  $z_s$ , due to the difference between the liquid and solid free energies,  $-\delta\omega_{\text{sub}}^{2D}(\mu_s, T) > 0$  (we have written the additional argument  $T$  in  $\delta\omega_{\text{sub}}^{2D}$  to make explicit its temperature dependence). Subtracting as in (59) the infinite contribution from the solid phase, this energy becomes  $-[(z_s - z^*)/d]\delta\omega_{\text{sub}}^{2D}(\mu_s, T)$ , with  $z^*$  an irrelevant constant. The remaining contribution to the soliton energy is due to the interface  $E_{\text{sl}}(z_s)$ , i.e., the non-constant part of the order-parameter profile, and consists of both potential,  $\delta\omega_{\text{sub}}^{2D}$ , and elastic,  $\propto (\mu'_z)^2$ , energies. Combining these two terms, we find (see Eq. (40))

$$\begin{aligned} E_{\text{sl}}(z_s) &= \frac{\ell T}{d} \int_{\mu_0^{\text{sl}}(z_s)}^{\mu_s} d\mu \sqrt{\frac{2\delta\omega_{\text{sub}}^{2D}(\mu)}{T}} \\ &= E_{\text{sl}} - \frac{\ell T}{d} \int_0^{\mu_0^{\text{sl}}(z_s)} d\mu \sqrt{\frac{2\delta\omega_{\text{sub}}^{2D}(\mu)}{T}} \\ &\approx E_{\text{sl}} - \sqrt{6(1 - \bar{c}_c)} T \frac{\ell [\mu_0^{\text{sl}}(z_s)]^2}{2}. \end{aligned} \quad (61)$$

In the last line of (61) we have expanded the 2D potential for small values of  $\mu$ . Since for a finite  $z_s$  the soliton has not fully entered in the system, its energy is less than the total soliton energy  $E_{\text{sl}}$  in (39) due to the missing tail, see Fig. 8. One sees that, whereas  $E_{\text{sl}}$  penalizes the entrance of the soliton and thus favors the solid phase,  $E_{\text{surf}}$  promotes the formation of the liquid phase at the surface. Combining all terms, we obtain the soliton energy (59)

$$\begin{aligned} E_{\text{sl}}^{\text{surf}}(z_s) &\approx E_{\text{sl}} + \frac{l}{\bar{\rho}} \frac{T_m - T}{T_m} z_s \\ &\quad + \frac{\ell T_m}{2d} \left[ \ell G - \sqrt{6(1 - \bar{c}_c)} \right] [\mu_0^{\text{sl}}(z_s)]^2, \end{aligned} \quad (62)$$

where we have expanded the solid free energy term about  $T_m$ ,  $\delta\omega_{\text{sub}}^{2D}(\mu_s, T) \approx \partial_T \delta\omega_{\text{sub}}^{2D}(\mu_s, T_m)(T - T_m)$  and we have used the definition of the latent heat  $l = T_m \Delta s = -(\bar{\rho}/d)T_m \partial_T \delta\omega_{\text{sub}}^{2D}(\mu_s, T_m)$ .

Below melting, the term  $\propto z_s$  forbids the entry of the soliton into the bulk. At the melting transition  $T_m$ , the third term plays the crucial role with a finite order parameter at the surface  $\mu_0^{\text{sl}}(z_s)$  leading to a positive or a negative energy contribution depending on the sign of the prefactor  $\propto [\ell G - \sqrt{6(1 - \bar{c}_c)}]$ . For a positive value ( $\ell G > \sqrt{6(1 - \bar{c}_c)}$ ), the minimal energy is achieved by  $\mu_0^{\text{sl}}(z_s) = 0$ . As a consequence, the soliton enters completely inside the sample at  $T_m$  (surface melting). On the other hand, for  $\ell G < \sqrt{6(1 - \bar{c}_c)}$ , the entry of the interface costs a positive energy and, thus, the soliton remains pinned at the surface at  $T_m$ . The two different behaviors are separated by the multicritical point, whose location is given by

$$\ell(T_{\text{mc}}, B_{\text{mc}})G(B_{\text{mc}}) = \sqrt{6(1 - \bar{c}_c)}. \quad (63)$$

This equation coincides with (57).

The appearance of the multi-critical point  $(T_{\text{mc}}, B_{\text{mc}})$  along the melting line can be interpreted as a surface-depinning transition of the solid-liquid interface (soliton). To find the precise pinning location of the soliton in the  $O_1$  regime a more detailed analysis is required, accounting for the higher order terms in (61). We have calculated this potential numerically in both the surface melting and surface non-melting regimes, using the following scheme: we place a bulk soliton at different distances from the surface and evaluate numerically the total non-local energy (29) as a function of  $z_s$ . In Fig. 9, we present two different curves, one at  $T = 0.33 \varepsilon_0 d > T_{\text{mc}}$  and another at  $T = 0.28 \varepsilon_0 d < T_{\text{mc}}$ . While for higher temperatures the potential exhibits a stable minimum close to the surface where the soliton remains pinned, upon decreasing the temperature the minimum moves deeper into the bulk and disappears altogether at  $T_{\text{mc}}$ .

When the surface melts continuously, we can characterize the transition by specific critical exponents, cf. Ref. 18. In particular, we can look at how the soliton position  $z_s$  depends on  $T$ . Here, we need the function  $\mu_0^{\text{sl}}(z_s)$ , i.e., the relation between the value of the order parameter on the surface and the soliton position  $z_s$ . For a soliton which is well inside the sample,  $\mu_0^{\text{sl}}(z_s)$  can be approximated as (cf. (45))

$$\mu_0^{\text{sl}}(z_s) \approx e^{-G + \sqrt{r} z_s}. \quad (64)$$

The position of the soliton is found from the minimum of (62)

$$\begin{aligned} z_s(T) &\approx -\frac{1}{2G + \sqrt{r}} \ln \left[ \frac{\ell d(T_m - T)}{2\sqrt{r}G + \bar{\rho}\ell T_m^2(\ell G - \sqrt{6(1 - \bar{c}_c)})} \right] \\ &\sim 0.5\ell \left| \ln[(1 - T/T_m)/(\ell G - \ell G|_{\text{mc}})] \right|. \end{aligned} \quad (65)$$

Hence, the soliton slides into the system logarithmically<sup>12</sup> with  $T \rightarrow T_m$ . Next, we study how the residual order parameter on the surface goes to zero. Combining (65) together with (64), we find that

$$\mu_0(T) \sim (1 - T/T_m)^{1/2}. \quad (66)$$

These results are standard in the theory of surface melting when only short-range interactions are present<sup>12</sup>.

For a continuous surface-melting transition the soliton propagates into the bulk at  $T_m$ , leading, in a semi-infinite system, to the coexistence of the liquid and the solid. The interface deep in the bulk produces the maximum free energy cost,  $E_{\text{sl}}^{\text{surf}}(z_s \rightarrow \infty) = E_{\text{sl}}$  (see Sec. IV B). This energy is only an interface energy and, hence, its contribution vanishes in the thermodynamic limit. In realistic finite systems, one has to account for the effect of the opposite surface. Approaching  $T_m$  from below, both surfaces undergo a continuous melting transition. The two surfaces act like two nucleation points for the liquid phase, giving rise to two opposite solitons. The system is then composed of a sequence of liquid-solid-liquid regions. At  $T_m$  the two solitons merge and the intermediate solid domain vanishes altogether. Hence, the solid cannot be overheated above the melting temperature.

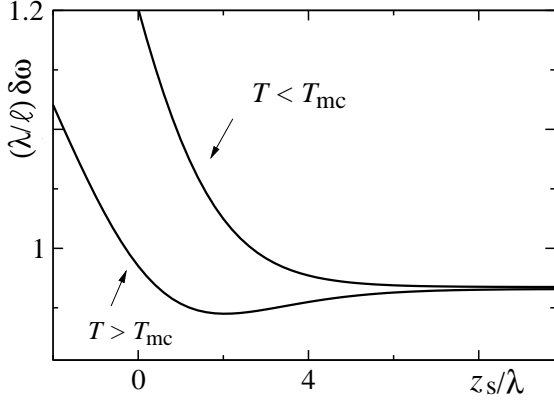


FIG. 9: Energy as a function of the soliton position  $z_s$ . Note the minimum for  $T = 0.33 \varepsilon_0 d > T_{mc}$  ( $O_1$ , pinned soliton) which has disappeared at  $T = 0.28 \varepsilon_0 d < T_{mc}$  ( $O_2$ , depinned soliton).

## VI. NUMERICAL ANALYSIS

In order to check the accuracy of our analytical approach, we have carried out a numerical solution of the saddle-point equations (42). As a preliminary step, we write (42) in a slightly different form which is more convenient for our numerical study. From (18), we obtain that at the saddle-point the solutions for  $\xi_z$  and  $\mu_z$  are related by

$$\xi_z = \int_0^\infty \frac{dz'}{d} \bar{c}_{z,z'} \mu_{z'}. \quad (67)$$

Combining this expression with the relation (cf. (24))

$$\mu_z = \Phi'(\xi_z)/6, \quad (68)$$

where the function  $\Phi$  is defined in (25), we obtain a set of integral equations which determine the order-parameter profile  $\mu_z$

$$6\mu_z = \frac{\int_v d^2\mathbf{R} g(\mathbf{R}) \exp\left[\int_0^\infty \frac{dz'}{d} \bar{c}_{z,z'} \mu_{z'} g(\mathbf{R})\right]}{\int_v d^2\mathbf{R} \exp\left[\int_0^\infty \frac{dz'}{d} \bar{c}_{z,z'} \mu_{z'} g(\mathbf{R})\right]}, \quad (69)$$

where we have written  $\Phi'$  explicitly. Our numerical solution is based on the recursive solution of (69).

We first discretize the  $z$  axis in  $N = 1000$  values  $\{z_i\}$  with a fixed distance  $z_i - z_{i-1} = \Delta z = 0.04 \lambda$  (for  $\Gamma > 40$  we use a smaller step size  $\Delta z = 0.01 \lambda \approx d$ , since the soliton interface becomes sharper). We start from a constant solid phase and initialize the values of  $\{\mu_i\}$  as  $\mu_i = \mu_{z_i} = \mu_s$ , for any  $i$ . Then, from Eq. (67), we derive the molecular field profile  $\xi_i$  in correspondence to the values  $\{z_i\}$ . We calculate the RHS of equation (68) for  $i = 1, \dots, i_{\max}$ , while keeping the last values ( $i = i_{\max} + 1, \dots, 1000$ ) unchanged, and obtain the new  $\mu_i^n = 6\Phi'(\xi_{z_i})$ . We compare  $\{\mu_{z_i}^n\}$  with

$\{\mu_{z_i}\}$  and if both the inequalities  $\mu_0^n - \mu_0 < 10^{-5}$  and  $(1/N) \sum_i (\mu_{z_i}^n - \mu_{z_i}) < 10^{-5}$  are satisfied, we accept  $\{\mu_{z_i}^n\}$  as the order-parameter profile. Otherwise, the procedure is iterated recursively until a stable solution (fixed point) is reached. We take  $i_{\max} = 750$ ; for this value we have checked that the connection between the numerical solution for  $i \leq i_{\max}$  and the constant bulk value for  $i > i_{\max}$  is smooth (we find a small jump at  $i_{\max}$ ,  $(\mu_{i_{\max}+1} - \mu_{i_{\max}})/\mu_{i_{\max}} \approx 10^{-5}$ ). Usually convergence is obtained after a reasonable number of iteration ( $< 100$ ), however in the proximity of a continuous surface transition the convergence becomes slow. This critical slowing down makes it difficult to track the sliding of the soliton inside the bulk. To avoid this problem, for these critical cases we start our iteration from a more convenient initial state. Instead of initiating the profile in the bulk homogenous solid, we chose to start from a bulk soliton at the position which minimizes the total surface free energy (cf. Fig. 9 and discussion in the last section). In this case the convergence is extremely rapid.

In Figs. 10 and 11, we show two different examples of the order-parameter profile for two different values of the temperature: *i*)  $T = 0.08 \varepsilon_0 d < T_{mc}$  in Fig. 10, where the surface undergoes a continuous transition and *ii*)  $T = 0.33 \varepsilon_0 d > T_{mc}$  in Fig. 11 where a discontinuous surface transition takes place. For the  $O_2$  transition at  $T = 0.08 \varepsilon_0 d$ , we show the order-parameter profiles for different values of the magnetic field  $B$ , increasing from top to bottom. At low magnetic fields, the profile is almost constant (cf. the topmost line), since the surface kernel  $\delta\omega^s$  is negligible and the system is translationally invariant. Going to larger values of the magnetic field, the modifications of the interlayer potential on the surface become relevant, reducing the value of the order parameter at the surface. Upon increasing the magnetic field further towards the thermodynamic melting transition, the vortex density modulation becomes vanishingly small close to the surface. The numerical solution shows that the order parameter at the surface goes to zero (liquid) continuously. Hence, the surface assists the penetration of the liquid phase by the formation of a quasi-liquid nucleus. This continuous transition on the surface eliminates the hysteresis above the melting transition, by preventing the appearance of a metastable overheated solid phase.

At larger temperatures  $T = 0.33 \varepsilon_0 d > T_{mc}$  (Fig. 11), the surface undergoes a discontinuous transition, although with a reduced jump in comparison with the bulk. Again starting from low magnetic fields (topmost line) the order parameter is constant, due to the smallness of the surface destabilizing potential. Increasing  $B$ , the value of  $\mu_0$  decreases, still showing a larger suppression than in the bulk. However, the surface potential is not strong enough to push  $\mu_0$  to zero and at melting (thick line) the surface still exhibits a finite order parameter. The transition to the homogeneous liquid phase then occurs via a finite global jump including the surface value  $\mu_0$  as well. This discontinuous transition is compatible

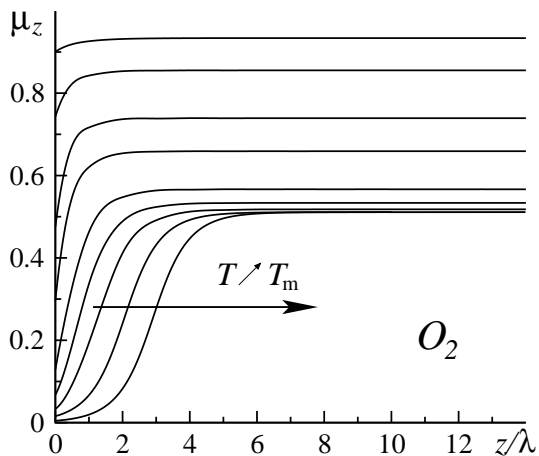


FIG. 10: Numerical solutions of the order-parameter profile  $\mu_z$  at the surface, for different values of the external magnetic field at  $\Gamma = 2\varepsilon_0 d/T = 25$ , corresponding to  $T = 0.08\varepsilon_0 d$ . At this temperature the bulk melts at  $B_m/B_\lambda \approx 0.1528$ . The lines from top to bottom correspond to the magnetic fields with values  $B/B_\lambda = 0.01, 0.05, 0.1, 0.125, 0.145, 0.15, B_m/B_\lambda - 10^{-4}, B_m/B_\lambda - 10^{-5}, B_m/B_\lambda - 10^{-6}$ . While approaching this value the soliton slides into the bulk (see the bottom three lines). The surface undergoes an  $O_2$  type transition, i.e.,  $\mu_0$  approaches zero (liquid phase) continuously.

with the appearance of the metastable phase. Indeed, numerically it is possible to obtain a non-uniform solution even at magnetic fields which are larger than the freezing field (lowest line in Fig. 11).

Finally, we check the accuracy of our analytical approach in estimating the location of the multi-critical point  $(T_{mc}, B_{mc})$ . We plot the residual value of the surface order parameter at melting as a function of temperature in Fig. 7, together with the solution of (56). For a continuous surface melting transition the order parameter is exactly zero at melting. Numerically, we associate the value  $\mu_0 = 0$  to situations where the soliton potential does not show a stable minimum as a function of  $z_s$  (see Fig. 9). Otherwise, we estimate the finite value of  $\mu_0$  within the iterative solution of the saddle point equations, which we have described above. The agreement of the numerical and analytical results is excellent, in particular in the vicinity of the multi-critical point.

## VII. CONCLUSIONS

In this paper, we have analyzed the impact of an *ab*-surface on the melting transition of the pancake vortex lattice. We have adapted the DFT-substrate approach<sup>22</sup> to include the presence of the surface. We have found that for intermediate values of the magnetic field, the surface undergoes a continuous melting transition and assists a smooth propagation of the liquid into the bulk. This result reveals the origin of the asymmetric hysteresis at the melting transition observed by Soibel *et al.*<sup>7</sup> as

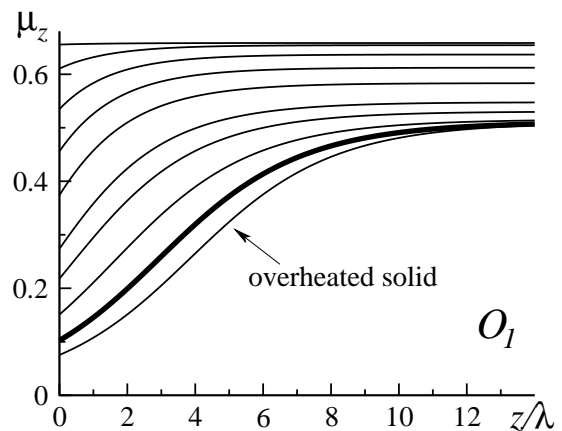


FIG. 11: Numerical solutions of the order-parameter profile  $\mu_z$  near the surface at  $T = 0.33 \varepsilon_0 d$  ( $\Gamma = 6$ ) for different values of the magnetic field. The freezing field is  $B_m/B_\lambda \approx 0.002396$  (thicker line). The lines from top to bottom correspond to the magnetic fields with values  $B/B_\lambda = 0, 0.0001, 0.0005, 0.001, 0.0015, 0.002, 0.0022, 0.00235, B_m/B_\lambda, B_m/B_\lambda + 10^{-5}$ . The order parameter at the surface jumps discontinuously to zero; hence, the surface transition is in the class  $O_1$ . In this case, the surface does not preclude the appearance of the overheated solid. Numerically it is possible to obtain a non uniform solution even at magnetic fields  $B > B_m$  larger than the freezing one (cf. lowest thin line), corresponding to a metastable configuration (overheated solid).

the consequence of free surfaces which can act as nucleation sites for the liquid phase. Moreover, we have found that at low and high magnetic fields the surface transition turns discontinuous as in the bulk. The continuous and discontinuous transitions at the surface are separated by a multi-critical point. While the precise location of the high-field multi-critical point goes beyond the limits of validity of our analysis, we have determined the position of the low-field multi-critical point by means of an analytical solution of the DFT equations and numerically confirmed the result of our analysis.

An effect which we have not included in our study is the impact of the reentrance of the melting line at low magnetic fields. At low magnetic fields the interaction between full *vortex lines* is strongly screened. This leads to a softening of the vortex lattice with exponentially small shear and compression moduli and to the reentrance of the melting line towards small temperatures. The effect of a surface in this reentrant low-field regime is an interesting problem as well. The stray magnetic fields produce an algebraic interaction between the tips of the vortex lines<sup>30</sup> instead of the exponentially small bulk interaction. This may lead to a highly unconventional scenario (proposed in Ref. 41) where the tips of the vortex lines on the surface are arranged in a regular lattice while the vortex system is already melted in the bulk. Hence, in this case the surface plays a role which is opposite to the one played in the standard surface melting scenario, since it favors the appearance of

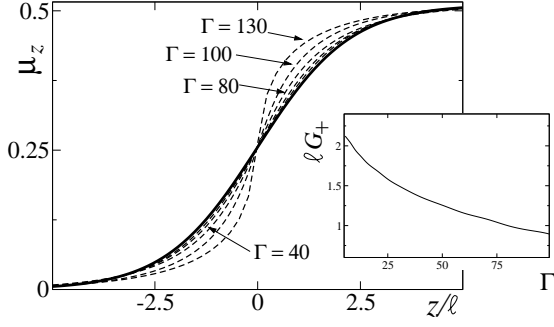


FIG. 12: Comparison of the soliton derived within the local approximation (thicker line) with the results of the full non-local theory for different values of  $\Gamma = 6, 40, 80, 100, 130$ . For  $\Gamma = 6$ , upon rescaling  $z$  in units of  $\ell$ , the soliton collapses on the solution of the local approximation. Little deviations are present at  $\Gamma = 40$ , where the soliton is still well approximated by the gradient expansion. At higher  $\Gamma$ 's the difference is appreciable: the full non-local theory leads to a sharper interface. Inset: plot of the ratio between  $\ell$  and kernel extension  $1/G_+$  as a function of  $\Gamma = 2\varepsilon_0 d/T$ . Assuming that the gradient expansion is valid for  $\ell_e G_+ \approx 4\ell G_+ \gtrsim 5$ , we obtain the limiting value  $\Gamma \approx 50$ , corresponding to  $T \approx 0.04 \varepsilon_0 d$ .

the solid instead of the liquid. The impact of this ‘surface solidification’ on our results remains an interesting open question.

We acknowledge support from the Swiss National Foundation through MaNEP (ADC) and from the DST (India) through a Swarnajayanti Fellowship (GIM).

## APPENDIX A: GRADIENT EXPANSION

### 1. Kernel in Fourier space

In this Appendix we test the validity of the gradient expansion (36) for the DFT free energy in the low-field regime. We start from the expression of the bulk free energy (33) and calculate the saddle point equation

$$-6\bar{\alpha} \int \frac{dz'}{d} \bar{f}_{z-z'}(\mu_z - \mu_{z'}) = \partial_{\mu_z} \delta\omega_{\text{sub}}^{2D}(\mu_z)/T, \quad (\text{A1})$$

which has to be compared with the corresponding equation (38) originating from the approximated local theory. The difference between the two left-hand side terms of (A1) and (38) is more conveniently analyzed in Fourier space. In the case of the local theory, the second derivative term is diagonal in Fourier space and its components read

$$\ell^2 k^2 \mu_k. \quad (\text{A2})$$

In the full non-local theory, the left hand side of (A1) is also diagonal in Fourier space

$$6\bar{\alpha}(\bar{f}_k - \bar{f}_{k=0})\mu_k = \frac{\ell^2 k^2}{1 + (k/G_+)^2} \mu_k, \quad (\text{A3})$$

where we have used  $\ell = 12\bar{\alpha}/dG_+^3$ , cf. (37). From the comparison of (A3) with (A2) it becomes clear that for small wave numbers  $k \ll G_+$ , i.e., for variations on scales larger than  $1/G_+$ , the gradient expansion approximates well the full non local theory. A convenient test is to compare the typical length of the soliton  $\ell_e \approx 4\ell$  (cf. (41)) with the size of the kernel  $1/G_+$ . If we choose  $\ell_e G_+ \approx 5$  as the limiting value for the validity of the expansion, we obtain that for  $\Gamma \lesssim 50$  (corresponding to  $T \gtrsim 0.04 \varepsilon_0 d$  or  $B \lesssim 0.5 B_\lambda$ ) the gradient approximation is justified, see the inset of Fig. 12. Expanding (A3) to second order, we find that the maximum error is only few percent,  $(k/G_+)^2 \approx 1/(\ell_e G_+)^2 \lesssim 0.04$ . To confirm this result we have solved numerically the integral equation (A1) imposing the boundary conditions  $\mu_{z \rightarrow -\infty} = 0$  and  $\mu_{z \rightarrow \infty} = \mu_s$ . The results for different values of  $\Gamma$  are plotted in Fig. 12, together with the soliton of the local theory (thick line). We have rescaled the  $z$  axis in units of the elastic length  $\ell$ . For  $\Gamma < 80$  we obtain a good collapse of the data. On the other hand, for large  $\Gamma$  the kink in non-local theory is sharper than the soliton in the local theory and, therefore, the gradient expansion approximates poorly the exact result.

### 2. Linearised saddle-point equation

For small values of  $\mu_z$ , we can expand the potential in the RHS of the equation (A1). Hence, we write, cf. (46),

$$\partial_{\mu_z} \delta\omega_{\text{sub}}^{2D}(\mu_z)/T \approx 6(1 - \bar{c}_c)\mu_z, \quad (\text{A4})$$

where we consider the system at melting, i.e.,  $c_{\text{sub}}^{2D} = \bar{c}_c$  to connect with the discussion in Sec. VB. Inserting (A4) and (A3) in (A1), we obtain the equation of ‘motion’ in Fourier space

$$-\ell^2 k^2 \left[ 1 + \frac{6(1 - \bar{c}_c)}{(\ell G_+)^2} \right] \mu_k = 6(1 - \bar{c}_c)\mu_k. \quad (\text{A5})$$

We can transform this equation back to real space

$$(1 + r)\ell^2 \mu_z'' = 6(1 - \bar{c}_c)\mu_z, \quad (\text{A6})$$

where we have defined the parameter  $r = dG_+(1 - \bar{c}_c)/2\bar{\alpha} = 6(1 - \bar{c}_c)/(G_+\ell)^2$ , as in Eq. (51). The higher derivatives which are neglected in the gradient expansion produce a small renormalization of the elastic term  $(1 + r) \approx 1$ .

- 
- <sup>1</sup> D. R. Nelson, Phys. Rev. Lett. **60**, 1973 (1988).
  - <sup>2</sup> A. Houghton, R. A. Pelcovits, and A. Sudbø, Phys. Rev. B **40**, 6763 (1989).
  - <sup>3</sup> E. H. Brandt, Phys. Rev. Lett. **63**, 1106 (1989).
  - <sup>4</sup> S. Sengupta, C. Dasgupta, H. R. Krishnamurthy, G. I. Menon, and T. V. Ramakrishnan, Phys. Rev. Lett. **67**, 3444 (1991).
  - <sup>5</sup> E. Zeldov, D. Majer, M. Konczykowski, V. B. Geshkenbein, V. M. Vinokur, and H. Shtrikman, Nature **375**, 373 (1995).
  - <sup>6</sup> A. Schilling, R. A. Fisher, N. E. Phillips, U. Welp, D. D. W. K. Kwok, and G. W. Crabtree, Nature **382**, 791 (1996).
  - <sup>7</sup> A. Soibel, E. Zeldov, M. Rappaport, Y. Myasoedov, T. Tamegai, S. Ooi, M. Konczykowski, and V. B. Geshkenbein, Nature **406**, 282 (2000).
  - <sup>8</sup> A. De Col, G. I. Menon, V. B. Geshkenbein, and G. Blatter, Phys. Rev. Lett. **96**, 177001 (2006).
  - <sup>9</sup> M. J. W. Dodgson, A. E. Koshelev, V. B. Geshkenbein, and G. Blatter, Phys. Rev. Lett. **84**, 2698 (2000).
  - <sup>10</sup> A. R. Ubbelohde, *The Molten State of Matter* (Wiley, New York, 1978).
  - <sup>11</sup> L. Pietronero and E. Tosatti, Solid State Commun. **32**, 255 (1979).
  - <sup>12</sup> R. Lipowsky, Phys. Rev. Lett. **49**, 1575 (1982).
  - <sup>13</sup> J. W. M. Frenken and J. F. van der Veen, Phys. Rev. Lett. **54**, 134 (1985).
  - <sup>14</sup> A. Trayanov and E. Tosatti, Phys. Rev. Lett. **59**, 2207 (1987).
  - <sup>15</sup> U. Tartaglino, T. Zykova-Timan, F. Ercolessi, and E. Tosatti, Physics Reports - Review Section of Physics Letters **411**, 291 (2005).
  - <sup>16</sup> A. Trayanov and E. Tosatti, Phys. Rev. B **38**, 6961 (1988).
  - <sup>17</sup> R. Ohnesorge, H. Löwen, and H. Wagner, Phys. Rev. E **50**, 4801 (1994).
  - <sup>18</sup> R. Lipowsky and W. Speth, Phys. Rev. B **28**, 3983 (1983).
  - <sup>19</sup> T. V. Ramakrishnan and M. Yussouff, Phys. Rev. B **19**, 2775 (1979).
  - <sup>20</sup> G. I. Menon, C. Dasgupta, H. R. Krishnamurthy, T. V. Ramakrishnan, and S. Sengupta, Phys. Rev. B **54**, 16192 (1996).
  - <sup>21</sup> P. S. Cornaglia and C. A. Balseiro, Phys. Rev. B **61**, 784 (2000).
  - <sup>22</sup> A. De Col, G. I. Menon, and G. Blatter, Phys. Rev. B, submitted BW10149.
  - <sup>23</sup> W. A. Curtin, Phys. Rev. B **39**, 6775 (1989).
  - <sup>24</sup> J. R. Clem, Phys. Rev. B **43**, 7837 (1991).
  - <sup>25</sup> J. R. Clem, J. Supercond. **17**, 613 (2004).
  - <sup>26</sup> V. Pudikov, Physica C **212**, 155 (1993).
  - <sup>27</sup> R. G. Mints, V. G. Kogan, and J. R. Clem, Phys. Rev. B **61**, 1623 (2000).
  - <sup>28</sup> A. De Col, V. B. Geshkenbein, and G. Blatter, Phys. Rev. Lett. **94**, 097001 (2005).
  - <sup>29</sup> G. Blatter, M. V. Feigel'man, V. B. Geshkenbein, A. I. Larkin, and V. M. Vinokur, Rev. Mod. Phys. **66**, 1125 (1994).
  - <sup>30</sup> J. Pearl, J. Appl. Phys. **37**, 4139 (1966).
  - <sup>31</sup> J. P. Hansen and I. R. McDonald, *Theory of Simple Liquids* (Academic Press, London, 1986).
  - <sup>32</sup> T. V. Ramakrishnan, Phys. Rev. Lett. **48**, 541 (1982).
  - <sup>33</sup> J. Chakrabarti, H. R. Krishnamurthy, and A. K. Sood, Phys. Rev. Lett. **73**, 2923 (1994).
  - <sup>34</sup> Following standard practice of liquid theory, we define the Fourier transform of  $c(\mathbf{q})$  with an explicit factor  $\bar{\rho}^{3D}$  (dimensionless Fourier transform)  $c(\mathbf{q}) = \bar{\rho}^{3D} \int d^3\mathbf{r} c(\mathbf{r}) e^{-i\mathbf{q}\cdot\mathbf{r}}$ .
  - <sup>35</sup> A. D. J. Haymet and D. W. Oxtoby, J. Chem. Phys. **74**, 2559 (1981).
  - <sup>36</sup> D. W. Oxtoby and A. D. J. Haymet, J. Chem. Phys. **76**, 6262 (1982).
  - <sup>37</sup> This term is absent in the gradient expansion of the bulk equation, the difference being due to the higher-order derivatives  $\partial_z^n \mu_z$  that are neglected in the gradient expansion (see Appendix A).
  - <sup>38</sup> P. G. de Gennes, *Superconductivity of Metals and Alloys* (Addison-Wesley Publishing Company, 1966).
  - <sup>39</sup> V. Mineev and K. Samokhin, *Introduction to unconventional superconductivity* (Gordon Breach, Amsterdam, 1999).
  - <sup>40</sup> Y. Singh, Physics Reports **207**, 351 (1991).
  - <sup>41</sup> D. A. Huse, Phys. Rev. B **46**, 8621 (1992).